Applied Surface Science 749 (2026) 167948

Contents lists available at ScienceDirect

Applied Surface Science

journal homepage: www.elsevier.com/locate/apsusc

Full Length Article

Structural relaxation in soda lime silicate glass below the glass transition temperature during ion exchange

Mattia Biesuz [a,b,*], Michele Cassetta [c], Levent Karacasulu [a,*], Adane M. Abebe [a], Maciej Oskar Liedke [d], Ahmed G. Attallah [d,e], Eric Hirschmann [d], Andreas Wagner [d], Sebastiano Mariazzi [f,h], Roberto S. Brusa [f,h], Vincenzo M. Sglavo [a,b,g]

[a] University of Trento Department of Industrial Engineering, Via Sommarive 9, 38123 Trento, Italy
[b] INSTM, Via G. Giusti 9, Firenze 50121, Italy
[c] Department of Engineering for Innovation Medicine, Strada le Grazie 15, 37134 Verona, Italy
[d] Helmholtz-Zentrum Dresden – Rossendorf, Institute of Radiation Physics, Bautzner Landstraße 400, 01328 Dresden, Germany
[e] Physics Department, Faculty of Science, Minia University, Minia 6159, Egypt
[f] Department of Physics, University of Trento, Via Sommarive 14, 38123 Trento, Italy
[g] Institute of Photonics and Nanotechnologies, National Research Council, Via alla Cascata, 56/C, 38123 Trento, Italy
[h] TIFPA/INFN Trento, via Sommarive 14, 38123 Povo, Trento, Italy

ARTICLE INFO

Keywords:
Chemical strengthening
Ion exchange
Medium range
PALS
Raman

ABSTRACT

Chemical strengthening based on ion exchange, IE, is a crucial process for improving the mechanical properties of glass through the formation of a surface residual compression layer. Herein, we investigate the IE of float soda lime silicate glass at temperatures from 380°C to 490°C, with a focus on how the medium-range structure evolves and its relation to stress-relaxation phenomena. Using positron annihilation lifetime and Raman spectroscopy, it is shown that the free volume is substantially reduced by potassium incorporation starting at the lowest IE temperature (380°C), while no changes are observed in the silicate ring structure or bonding angles. When the maximum compressive stress is achieved (430°C), the free volume and the positron lifetime reach a minimum. Moreover, the Raman bands shift, indicating a narrowing of the Si-O-Si bond angle in the vicinity of the alkali cations. The transition between the squeezed and relaxed configuration is sharp, suggesting the existence of two well-defined configurations of the silicate backbone. As the IE temperature further increases, the residual stresses relax. This is coupled with an increase in the free volume and a relaxation of the Si-O-Si bonding angles toward the original configuration. These results clarify that (i) the free volume shrinkage can partially account for the residual stress relaxation through a mechanism not involving a re-construction of the network; (ii) potassium can fill different types of sites accessible at different temperatures, with higher temperatures activating sites straining the silicate framework; (iii) stress relaxation at "high temperature" mirrors a relaxation of the medium-range structure.

1. Introduction

Silicate glasses are among the most widely used materials worldwide with various applications. They are also relevant in different sciences, including geology and volcanology [1,2]. In particular, soda lime silicate (SLS) glass is by far the most common composition and the most widely produced commercial glass worldwide and provides a well-established model system. One of the major processing techniques, Glass sheet production, relies on the float process, in which a viscous ribbon floats on a molten tin bath to produce flat plates of varying thickness. As tin diffuses into the glass network, the so-called "air side" (in contact with the atmosphere) and "tin side" (in contact with the molten metal) can be distinguished based on their chemistry, structure, and various properties. [3–14].

The intrinsic brittleness and propensity to surface damage make silicate glass typically weak from a mechanical point of view. Mechanical strength can be improved through thermal or chemical strengthening. Both approaches aim to introduce compressive residual stresses

* Corresponding author at: University of Trento Department of Industrial Engineering, Via Sommarive 9, 38123 Trento, Italy.
E-mail addresses: mattia.biesuz@unitn.it (M. Biesuz), levent.karacasulu@unitn.it (L. Karacasulu).

https://doi.org/10.1016/j.apsusc.2026.167948
Received 12 April 2026; Received in revised form 15 July 2026; Accepted 23 July 2026
Available online 24 July 2026

on the glass surface, where the largest flaws are typically located. Chemical strengthening was introduced in 1962 by Kistler [15] and Alloque-Tochon [16]. It relies on an ion exchange (IE) process [17]: the glass artifact is soaked in a molten bath containing monovalent cations, such as alkalis or silver, which exchange with sodium ions present in the glass, driven by the concentration gradient. Due to differences in ionic radius between Na^+ and the ions from the bath, surface compression occurs [18]. Chemical strengthening is typically carried out at a temperature of about 120–150°C below *Tg* to allow sufficient ion diffusion while preventing stress relaxation. This process can generate surface compression of approximately 400–700 MPa [19], with the compressive layer being a few tens of micrometers thick. At present, the optimization of IE can be achieved even via machine learning [20,21]. Besides glass, IE can also be applied to traditional ceramics [22–25] (containing an amorphous alkali-modified silicate matrix) and to some glass-ceramics [26,27].

Although IE is often described as a simple replacement of smaller alkali ions by larger ones, the process involves more complex structural and mechanical phenomena. Although IE creates significant compressive stress, the expansion achieved during ion exchange is typically lower than that expected from the molar volume difference between alkali end-member compositions, resulting in compressive stresses below the theoretical limit. This, commonly known as the network dilation anomaly, has been reported in the relevant studies of chemically strengthened glasses [28,29]. Molecular dynamics (MD) simulations have shown that the larger K^+ ions introduced during IE cannot achieve the same local environment as in an as-melted potassium glass, leading to incomplete network expansion [28]. This limited expansion can be related to the ability of glass network's ability to accommodate the imposed strain, which is tuned by network connectivity. As network connectivity increases, the structure becomes more rigid and tends to store strain as internal stress rather than macroscopic expansion [29]. No significant changes in Q^n speciation are observed; however, structural reorganizations occur in medium-range structural features, including alkali-ion environments, intertetrahedral Si-O-Si bond angles, and ring statistics [30,31]. In addition to qualitatively correlating Raman spectral changes to the ion-exchange profile and the compressive layer [32], these structural rearrangements are considered to determine even the development of residual compressive stress by micro-Raman spectroscopy [31,33]. Still, it is well known that surface compression achieved through chemical strengthening is typically only about 25–40% of what theoretical simulations suggest [17,19,34]. This indicates that some form of stress relaxation occurs at the ion exchange temperature (i.e., well below the glass transition temperature, *Tg*), leading to "irreversible deformation" [35,36] associated with shear/densification of the network. Nevertheless, the mechanisms underlying these phenomena are not yet fully mechanistically understood [17,19].

This work aims to better understand how the chemical strengthening process affects the silicate network in the most commonly used SLS glass on both the air and tin sides at the medium-range structure. In this context, free volume evolution was investigated by positron annihilation lifetime spectroscopy (PALS), whereas structural changes in silicate ring size/bonding angles were examined using Raman spectroscopy. The medium-range evolution is correlated with stress-relaxation phenomena using both spectroscopic methods.

2. Materials and methods

A commercial soda lime silicate float glass (SLS) sheet with a nominal thickness of 4 mm was cut into squares of about 2 × 2 cm^2 with a diamond cutter. The nominal composition provided by the manufacturer is (wt%): SiO_2 71.4%, Al_2O_3 1.0%, Na_2O 13.9%, K_2O 0.3%, MgO 4.1%, CaO 9.1%, and other 0.2%. The elemental distribution of the pristine glass and the SIMS depth profiles are provided in the Supplementary Material (Figs. S1&S2). The glass was then cleaned with acetone in an ultrasonic bath for 10 min. The air side (AS) and tin side (TS) of the glass were identified using a UV-C lamp to detect the characteristic luminescent features associated with the Sn incorporation in the network. The *Tg* of the glass is about 568°C, as previously determined by thermodilatometry [37].

The glasses were subjected to 4 h-long ion exchange in a molten potassium nitrate (Sigma Aldrich) bath pre-heated at different temperatures between 380°C and 490°C. The treatment was carried out in a stainless steel crucible.

After IE, the potassium incorporation was verified by energy-dispersive X-ray spectroscopy (EDXS). This was carried out both on the external surface of the IE glass and on its cross-section. Line-scan analysis were operated on the polished (grit 4000 SiC papers) cross-section of the tempered glasses to monitor the potassium profile. The analysis was carried out within a JEOL JSM 550 scanning electron microscope (SEM) operating at 20 keV. Before the analysis, the samples were coated with a thin Pt-Pd layer by sputtering.

The potassium diffusion was modelled using the typical law:

$$\frac{C_{(x)} - C_0}{C_S - C_0} = 1 - \mathrm{erf}\left(\frac{x}{2\sqrt{Dt}}\right) \quad (1)$$

where $C_{(x)}$ is the K concentration at depth x, C_0 and C_S the initial and surface concentration, D the interdiffusion coefficient and t the IE time. Herein, the concentrations were substituted by the EDXS counts for potassium, normalized on the silicon ones. This allows to reduce possible fluctuations in the EDXS counts induced by the surface topology.

These measurements were performed using a surface stress meter (FSM 60 LE, Tokyo, Japan) in accordance with the ASTM C1279 standard as a reference. For calculating the surface compression, a photoelastic constant equal to 25 × 10^{-6} MPa^{-1} was utilized.

The PALS measurements were carried out at the pulsed positron beam beamline, Mono-energetic Positron Source (MePS) at the ELBE (Electron LINAC for beams with high Brilliance and low Emittance) facility, Helmholtz-Zentrum Dresden-Rossendorf (HZDR), Germany [38]. 10^7 annihilation events were acquired in each spectrum. The annihilation gamma rays were detected by a $CeBr_3$ scintillator coupled to a Hamamatsu R13089-100 photomultiplier tube (PMT). The analog signals from the detector were digitized using a SPDevices ADQ14DC-2X digitizer [39]. The total time resolution of the system (pulsed beam and detector) was about 220 ps.

All the PALS spectra were recorded at a positron implantation energy of 12 keV, corresponding to a probed depth of approximately 0.8 μm, which basically represents the surface of the strengthened glass (the compressive layer is substantially thicker than this figure). Note that this thickness closely matches the probed surface region used to determine the maximum compression. The spectra, $F(t)$, included the sum of various exponential functions convoluted with a resolution function $r(t)$:

$$F(t) = r(t) \otimes \sum_i \frac{I_i}{\tau_i} e^{-\frac{t}{\tau_i}} + B \quad (2)$$

where τ_i and I_i are the lifetimes and the related intensities ($\sum_i I_i = 1$) and B the background. A resolution function including two Gaussian contributions was used. The deconvolution was carried out using the software PALSfit [40].

The PALS spectra could be modelled using three different lifetimes: a short lifetime (0.3–0.4 ns) representing annihilation in the bulk of the glass structure/small open volume (τ_2), and the two lifetimes correlated with the formation of the positronium bound state. The lifetime of the *para*-positronium (p-Ps) was fixed at 0.125 ns τ_1, while the *ortho*-positronium (o-Ps) pick-off lifetime was deconvoluted ($\tau_3 \approx 0.9$ ns). The intensity of the p-Ps annihilation event is typically about 1/3 of that of the o-Ps. The lifetime τ_3 is representative of the annihilations occurring in the free volumes of the network and can be correlated with the interstitial free volume size [41]. An effective free volume radius (r) was calculated from the o-Ps lifetimes reduced by pick-off by [42]

$$\lambda_{(r)} = \lambda_V \left(1 - \frac{r}{r+\Delta r} + \frac{1}{2\pi} \sin\left(\frac{2\pi r}{R+\Delta r}\right)\right) \quad (3)$$

where $\lambda_{(r)}$ is the inverse of the lifetime in free volume of radius r, $\lambda_V = (\lambda_S + 3\lambda_T)/4$ ps^{-1} with λ_S and λ_T are the annihilation rate of the singlet and triplet positronium state in vacuum, and $\Delta r = 0.16$ nm is an empirical parameter [42]. On the other hand, the intensity associated with the different lifetimes correlates with the number of annihilation events. Herein, we use I_2 / I_3 as a descriptor of the bulk/free volume annihilation events ratio.

Raman spectra were acquired using a Thermo Scientific DXR2 spectrometer equipped with a 532 nm solid-state laser. The scattered radiation was dispersed by a high-resolution grating (1800 grooves) and collected by a thermoelectrically cooled charge-coupled device (CCD). The grating covered the Stokes spectral region from 50 to 1875 cm^{-1}, providing an average spectral resolution of 1 cm^{-1}. The laser power at the sample surface was maintained at 10 mW by a 100x long working distance objective, and no evidence of laser-induced surface modification was observed before and after the measurement. To analyze each spectral contribution, the background was subtracted as a 2nd order polynomial in the range 200–1300 cm^{-1} (see Ref.[43] for details).

3. Results

The ion exchange process efficiently occurred in all the tested conditions, as evidenced by the EDXS analysis on the sample cross-section (Fig. 1(a,b)) and surface (Fig. 1(c)). Increasing the IE temperature causes a more intense potassium penetration on both AS and TS, although generally a slightly deeper exchange is noticed on AS (Fig. 1(a,b,d)). By fitting the experimental data with a complementary error function (Eq. (1)), it was possible to determine the diffusion distance ($2\sqrt{Dt}$) corresponding to the depth at which the potassium enrichment is about 16% of the surface one. We can observe that the surface concentration also generally increases with the IE temperature (Fig. 1(a–c)). In addition, the slightly higher K/Si ratio measured on the tin-side external surface was not confirmed by the cross-sectional analyses, suggesting that the apparent enrichment may arise from EDXS interaction-volume effects associated with the Sn-containing tin side.

The maximum residual compressive stress induced by chemical tempering is reported in Fig. 1(e) for the sample treated at temperatures exceeding 400°C. One can observe that the residual stresses were not measured below such a temperature because the compression layer was too thin to be evaluated by optical methods. The residual stresses peak at about 430°C (≈470–500 MPa), increasing the IE temperature, causing a modest relaxation up to 460°C (≈460–480 MPa), followed by a substantial drop when the IE is operated at 490°C (≈325–350 MPa). Both the air and tin sides follow a similar trend in the stress–temperature plot.

The PALS spectra show the typical exponential decay associated with the lifetime of the positron in the sample. Their evolution might seem modest (Fig. 2(a,b)); however, a clear trend can be observed in the deconvolution parameters (Fig. 2(c,d)). The IE causes a reduction in τ_3 already at 380°C with respect to the value at RT, which is associated with a substantial increase in I_2 / I_3. When the temperature further increases, the relative ratio between bulk/free volume annihilation mildly evolves. On the other hand, the lifetime continues to decrease up to 400–430°C. Starting from 460°C, τ_3 increases, but it does not reach the figure of the untreated material even at 490°C. This evolution in the o-Ps lifetime reflects the evolution in the free volume size (Fig. 2(e)), which shrinks up to 430°C: the size of the free volume before IE is about 0.295 nm (TS) – 0.298 nm (AS) and it drops to 0.277 nm (TS) – 0.282 nm (AS) at 430°C. Increasing the temperature above 430°C lead to an expansion in the free volume size. The average lifetime, $\tau_{av} = \sum_i \tau_i I_i$, which increases when the network is more open, substantially decreases when IE is carried out at 380°C (Fig. 2(f)). A marginal reduction in τ_{av} can still be detected up to 430°C; then, starting from 460°C, it mildly increases.

The said general evolution in the PALS spectra is observed both on AS and TS of the float glass. Nevertheless, some differences can be pointed out:

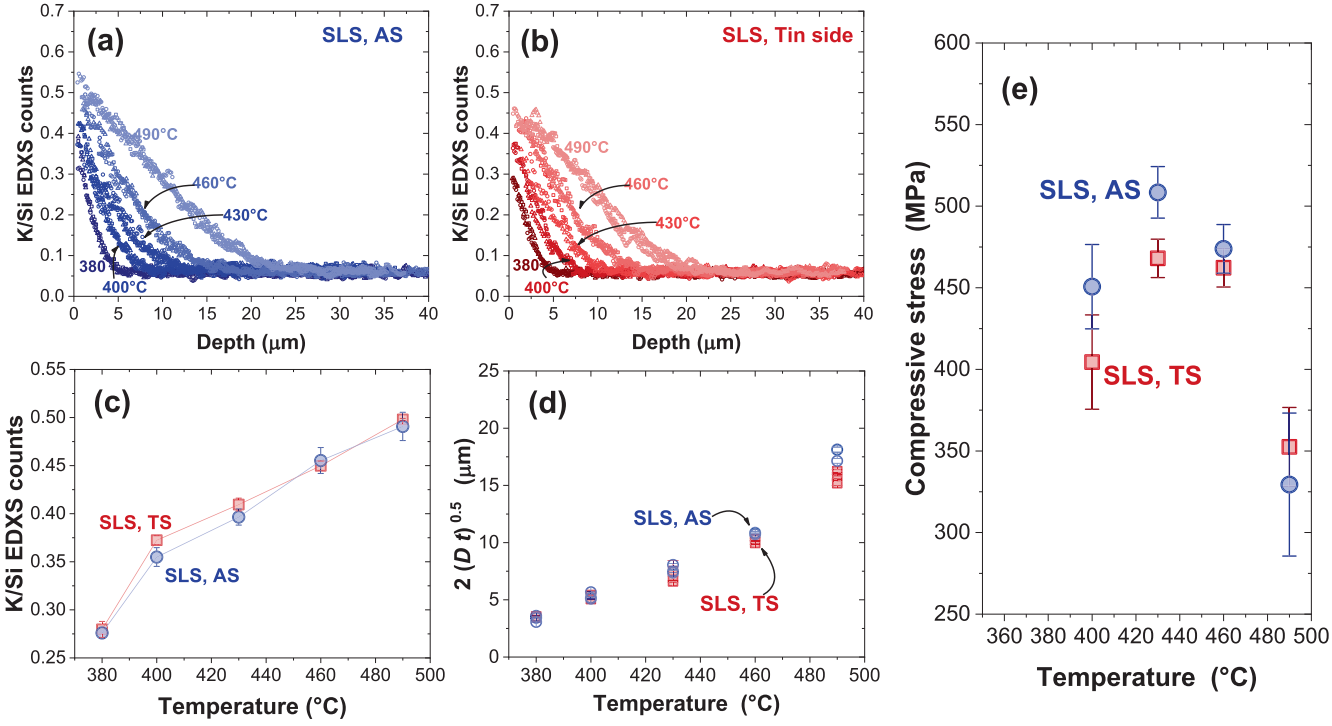

Fig. 1. EDXS K/Si counts from line scan analysis in the sample cross-section after IE at different temperatures on (a) AS and (b) TS. The surface is located at depth = 0. (c) reports the EDXS K/Si counts measured on the external surface. The diffusion distance (d) was measured by fitting the data in (a) and (b) with Eq.1. (e) Maximum surface compression determined by the surface stress meter.

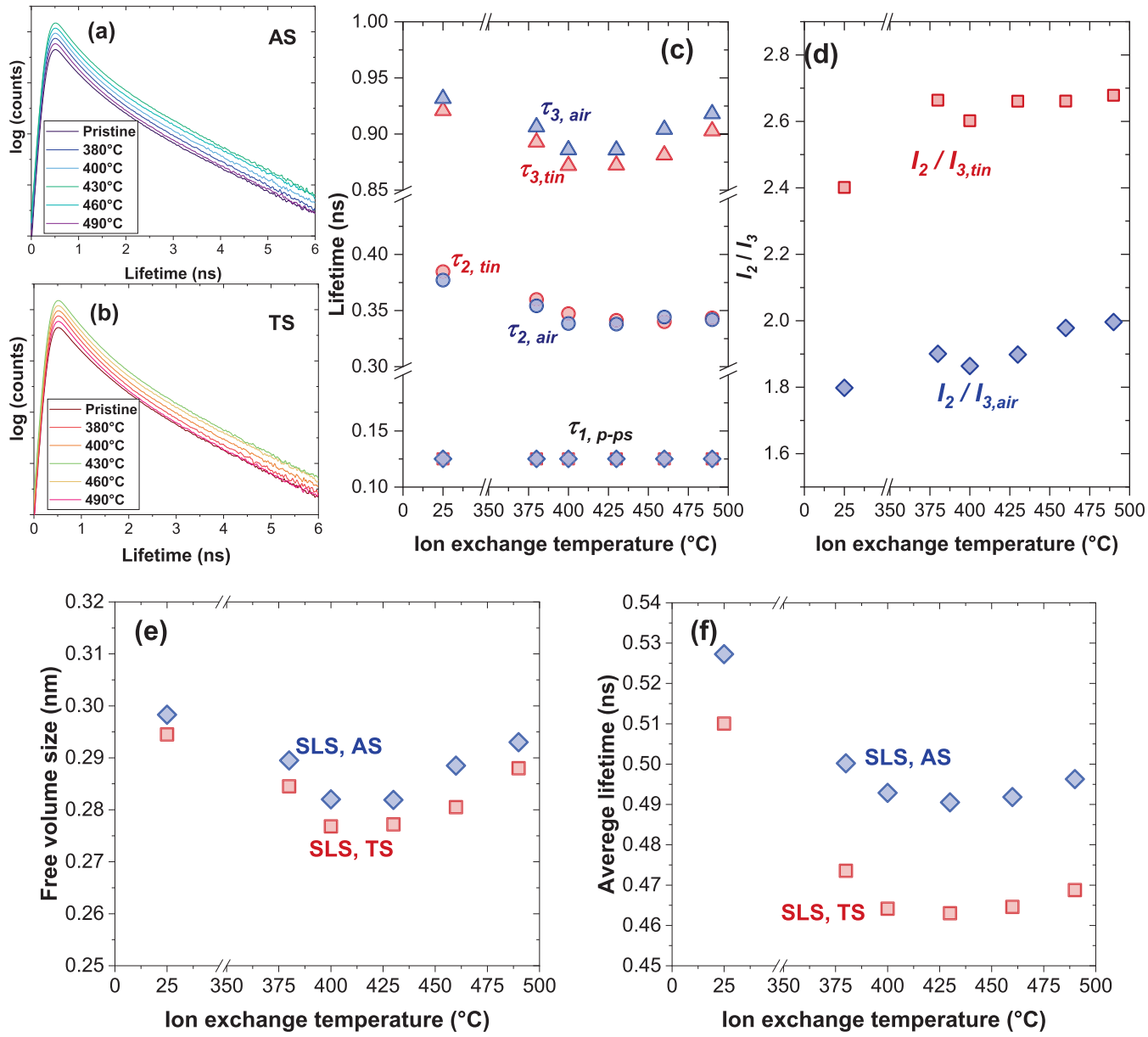

Fig. 2. PALS spectra obtained on (a) AS and (b) TS of the float glass before and after IE. Deconvolution parameters: (c) lifetime and (d) intensity of the spectra in (a, b). The error is always smaller than the marker's size. (e) Free volume size determined from the lifetime, τ_3, using Eq. (3). (f) Average lifetime, $\tau_{av} = \sum_i \tau_i I_i$, as a function of the IE conditions.

(i) TS is characterized by smaller free volumes, enhanced intensity in bulk annihilation, and shorter τ_{av}. This reflects a more compact network on the tin side, in coherence with previous results from the literature [44];
(ii) the τ_{av} increases above 430°C on the TS is slightly slower than on the AS.

Using the data in Fig. 2(e), it is possible to calculate the actual linear strain of the free volume during the IE process ($\varepsilon_{PALS} = \Delta r/r_0$, r_0 being the free volume radius in the untreated glass). This figure was compared with that expected from the elastic shrinkage of the network induced by the compressive stresses (data from Fig. 1(e)). To compute the elastic strain in the plane ($\varepsilon_{xx} = \varepsilon_{yy}$), we assumed a perfectly elastic isotropic material under plane stress ($\sigma_{xx} = \sigma_{yy}$):

$$\varepsilon_{xx} = \varepsilon_{yy} = \frac{\sigma_{xx}}{E\ (1\text{-}\nu)} = \frac{\sigma_{yy}}{E\ (1\text{-}\nu)} \quad (4)$$

The elastic modulus, E, and the Poisson ratio, ν, are assumed to be 70 GPa and 0.22, respectively. Fig. 3 shows the ratio between the actual strain of the free volume and the elastic one. The values are always well above 1, thus pointing out a free volume shrinkage abundantly surpassing the elastic one. The ratio between these strains can exceed 10 at 400°C, and decreases with the IE temperature.

The Raman spectra recorded on the sample surface (≈1 μm) are reported in Fig. 4(a,b) as a function of the IE temperature. The spectra contain the typical features of silicate glass:

(i) The symmetric stretching of the tetrahedral units dominates the 900–1200 cm^{-1} region with a major peak at about 1100 cm^{-1} connected with the Q^3 [45]. This portion of the spectrum is particularly sensitive to the short range and to the coordination of the metals in the tetrahedral units [46];
(ii) The Si-O-Si bending is visible in the region 750–850 cm^{-1} [47,48];

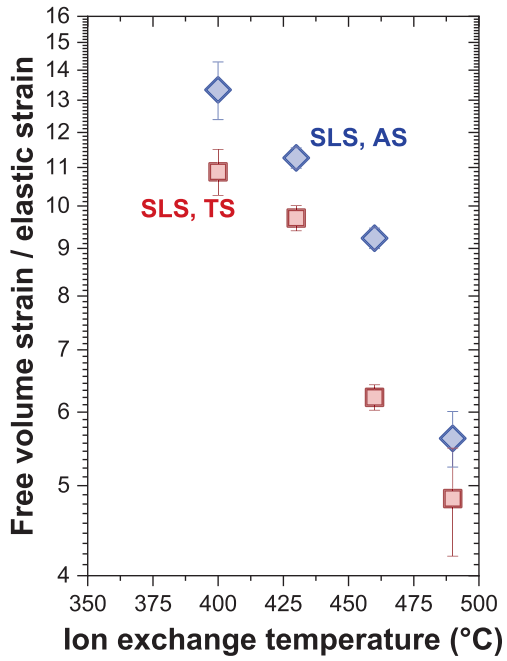

Fig. 3. Ratio between the actual free volume shrinkage (from the data in Fig. 2 (e)) and the elastic one computed using the residual stresses (Fig. 1(e)).

(iii) The low-frequency Raman region (200–750 cm^{-1}) is dominated by ring-breathing vibrations, which are commonly used as spectroscopic fingerprints of the medium-range organization of silicate glasses. However, these bands do not provide direct quantitative information on the population of rings with different sizes.. This portion of the spectrum includes the *R* band assigned to large rings, including at least 5 members, while no clear evidence of the D_1 and D_2 bands (4 and 3-fold rings, respectively) at 490 and 600 cm^{-1} can be observed 4950,51. This spectral region can be particularly sensitive to the Si-O-Si bonding angle, rings with larger bonding angles resonating at lower wavenumbers [49]. The band is broad as a result of the distribution of different geometries coexisting in an amorphous network. A clear *Rc* component in the low frequency can also be identified. This is a characteristic feature of alkali-containing glasses, where the local network geometry is "more ordered" in proximity to the modifiers [49]. This causes a relatively sharp spectral feature associated with a more defined Si-O-Si bonding angle.

The band-shape and position of the Raman features do not evolve when IE is carried out at 380°C. Conversely, a blue shift of the vibrational features occurs starting from 400°C, both on the air and on the tin side. While a substantial shift in all the main spectral features can be observed, the low-frequency region is the most interesting for our purposes, as a robust literature correlation exists between the breathing modes frequencies and the Si-O-Si bond angles. The *Rc* band, which at 380°C moves only by a couple of cm^{-1}, shifts at a higher frequency by 20–25 cm^{-1} at 400°C. Further increase in the IE temperature may cause

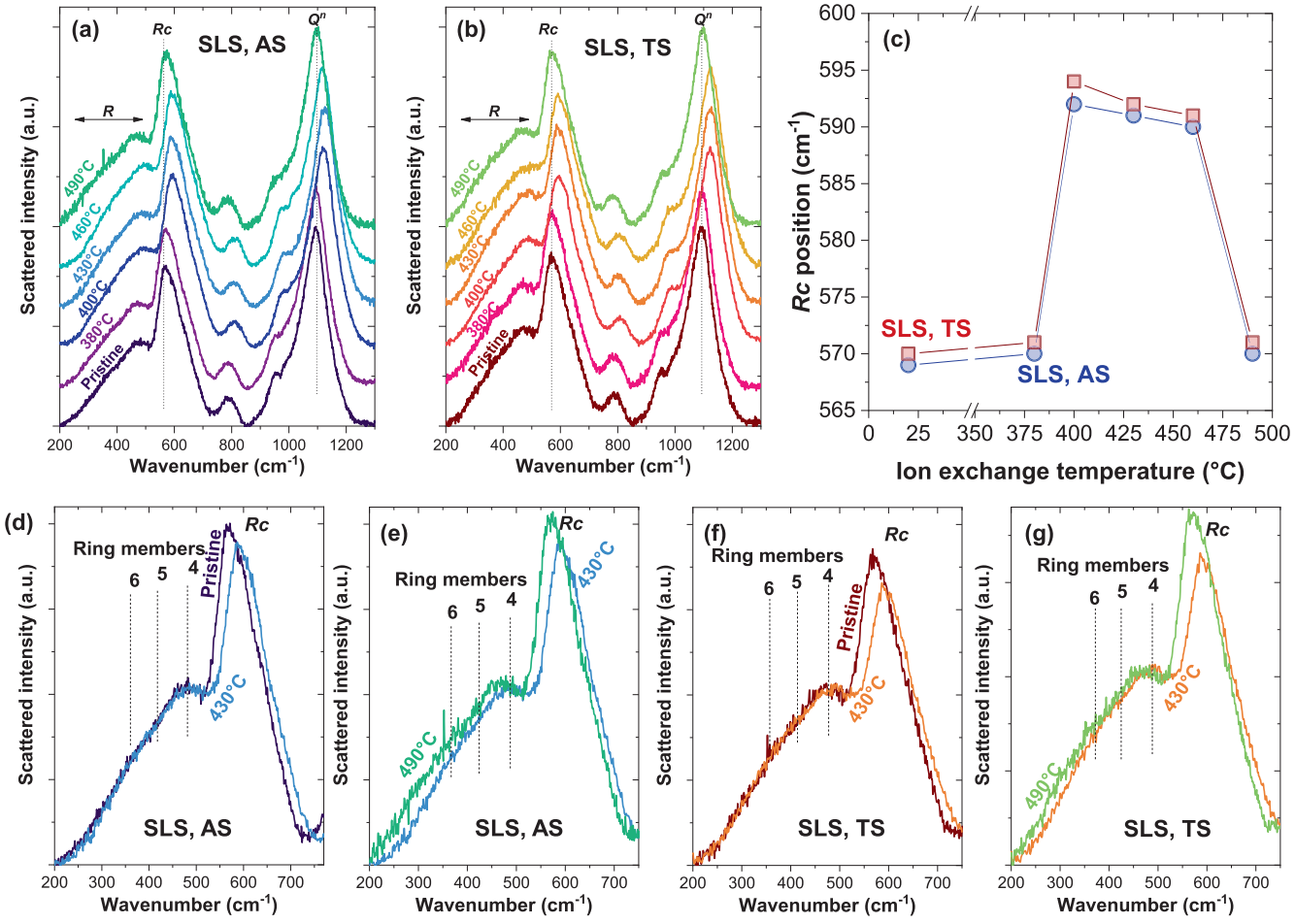

Fig. 4. Raman spectra collected on the sample's surface as a function of the IE temperature on (a) AS and (b) TS. The *Rc* band shift can be appreciated in (c). Magnification of the low-frequency portion of the spectra for IE samples are shown in (d,e) AS and (f,g) TS.

a modest relaxation in the *Rc* position at 430 and 460°C. When IE is carried out at 490°C, an almost complete relaxation can be noticed, and the *Rc* positions back to the wavenumbers of the pristine glass (Fig. 4 (c)). Said evolution in the *Rc* position is coupled with a modest but detectable dynamic also in its intensity: at 380°C the *Rc* intensity is unchanged, when the IE temperature increases (see for instance the spectrum at 430°C) the relative intensity of the *Rc* weakens; finally, at high temperature (e.g., 490°C) the *Rc* intensity increases again (Fig. 4(d, e,f,g)).

While starting from 400°C the *Rc* substantially shifts, no modification occurs in the shape and position of the *R* band (Fig. 4(d,f)). This can be noticed, for instance, by comparing the low-frequency Raman spectra of the pristine glass and of the SLS chemically tempered at 430°C. This specific temperature is reported just as an example, corresponding to the maximum compressive stress; similar conclusions could be obtained at 400°C. On the other hand, when IE is carried out at 490°C, the *Rc* relaxes back to the original position, but some changes occur in the low-frequency shoulder of the *R* band. Specifically, the sample treated at 490°C is characterized by a stronger intensity below 500 cm^{-1}, corresponding to large rings associated with higher Si-O-Si angles (Fig. 4(e, g)).

Fig. 5(a,b) shows the Raman spectra collected on the AS and TS ion exchanged at 490°C, focusing the laser beam at different depths within the sample. No shift in the vibrational features can be observed. On the other hand, a magnification of the low-frequency portion of the spectrum (Fig. 5(d,e)) points out a preference for large ring structures (i.e., the low Si-O-Si bonding angle region and low frequency) in proximity of the surface where the highest K content is achieved.

4. Discussion

These results suggest that the medium-range structure of the silicate network changes during the IE process. This evolution strongly correlates with the IE temperature, with the sites that potassium ions fill, and the developed residual stresses.

A first general observation is that the potassium ion concentration in the surface vicinity is temperature-dependent (Fig. 1(a,b,c)). Such a result is coherent with previous works; for instance, Erdem et al. showed an increase in the potassium surface concentration as the IE temperature increases [52]. Interestingly, they pointed out that the surface potassium concentration is time-independent (after an initial equilibration time) [52]. Similar results were also obtained by other authors, both by changing the IE time and temperature on different glass systems [53,54]. On these bases, we can infer that, during IE the potassium ions can sit in various environments with different coordination and site size; not all the sites appear accessible at a given temperature, and at higher IE temperature, the population of accessible sites for potassium increases. In summary, the chemical potential of potassium (and sodium) in the glass cannot be treated as a *unicum* due to the existence of different environments, each one possessing its own standard chemical potential. This concept could enrich the already existing extensive thermodynamic models of the IE process [55].

When the IE temperature is low (e.g., 380°C), potassium incorporation in the glass surface may not lead to deformation of the silicate network, but it can reduce the size and amount of free volume. In fact, already at 380°C, the average positron lifetime, the o-Ps lifetime, and the o-Ps intensity (*I3*) decrease significantly (Fig. 2(c,d,f)). These parameters may indicate a reduction of the amount and size of free volume in the network (Fig. 2(e)). This aligns with the fact that the ionic radius of K^+ is much larger than that of Na^+, and this volume difference is partly accommodated by reducing the network's empty space. In other words, the IE glass has a higher packing factor compared to the pristine material. One can note that the shrinkage of free volume cannot be explained by the elastic shrinkage of the bonding distance. In fact, the free volume's shrinkage can be an order of magnitude greater than the elastic one (Fig. 3). In summary, the decrease in free volume size might not be due to the established compression, but may depend on the filling by the large potassium ions.

The presented PALS results can contribute to the long-term discussion about the stress relaxation during chemical strengthening, the actual residual stresses being substantially lower than those theoretically calculated [17]. In fact, the free volume reduction during IE causes a reduction in the volume expansion of the network on the surface, the potassium ions' volume excess being accommodated in the empty space. Such a mechanism is intrinsically connected to the network structure and is not mediated by any time or temperature-dependent mechanism, like viscous flow. In other words, this relaxation mechanism is related to the structure and therefore the chemistry of the glass, rather than to the IE conditions, and cannot be eradicated by changing the chemical tempering parameters.

While the medium range, corresponding to the free volume, substantially evolves at 380°C, no changes in terms of silicate structure can be detected by Raman spectroscopy (Fig. 3). The glass structure appears to behave as a rigid framework within which the new ions are allocated.

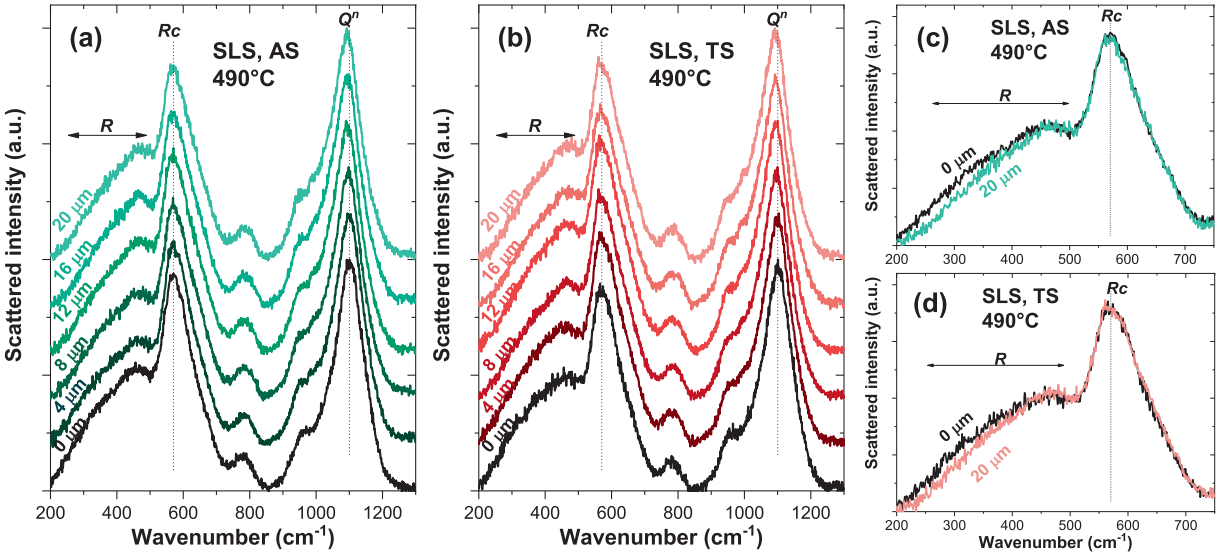

Fig. 5. Raman spectra collected on the sample's IE at 490°C at different depths beneath (a) AS and (b) TS surface. The changes in *R* and *Rc* spectral regions are magnified in (c) and (d).

This suggests that at 380°C the potassium ions fill pre-existing sites in the network with coordination that are compatible with the size of the potassium ions. Potassium in crystalline systems, like leucite, is usually 12-fold coordinated by oxygen; however, in melt-quenched K-containing silicate glasses, the coordination is generally lower, 9 or 10, as evidenced by XANES and neutron diffraction [56–58]. We can argue that these sites, existing in the parent glass structure, can easily accept potassium from the molten salt as they are thermodynamically more favorable.

At 400°C the free volume and the average positron lifetime continue to reduce (Fig. 2) while more potassium is incorporated on the glass surface (Fig. 1). However, at this temperature, the silicate network does not behave as a rigid framework anymore and a blue shift in the vibrational features occurs (Fig. 4). Looking at the low-energy portion of the Raman spectra, we can notice that this shift involves the *Rc* band while the *R* feature remains unchanged. Similar structural modifications are also recorded at 430°C, as shown in the magnified spectra in Fig. 4. This selective modification of the Raman features is coherent with the concept that the glass network presents some nanoscale separation between regions closer to a silica-like (responsible for the R band) and alkali-silicate-like structures (responsible for the *Rc*). The *Rc* shift at 400°C points out that the Si-O-Si bond angle is squeezed in proximity to the freshly introduced alkali ions (the alkali-silicate-like regions). Therefore, at 400°C, it can be assumed that potassium starts to fill smaller sites not matching its ideal coordination, causing a change in the bonding angles of the surrounding framework. The incorporation of K^+ in these smaller sites with reduced coordination compared to the melt-quenched glass has been already experimentally observed by Ragoen et al. by XANES [56]. In summary, the silicate network may behave as an "accordion" that is squeezed during ion exchange. This reduction of the bonding angles can contribute to said reduction in the free volume observed by PALS.

It is remarkable to observe that the transition in the *Rc* position is sharp, suggesting the existence of two well-defined configurations for the network: the relaxed one present in the pristine glass (*Rc* at about 570 cm^{-1}) and the stressed one obtained after ion exchange (*Rc* at about 590–595 cm^{-1}). We can finally note that the *Rc* intensity is partially reduced (see, for instance, the magnified spectra at 430°C, Fig. 4). This could originate from a disordering of the structure characterized by a larger dispersion in the bonding angles distribution induced by the potassium incorporation in smaller sites.

At 430°C, the maximum in the residual stress is achieved, with only very minor evolutions of the medium range structure compared with those already discussed at this temperature. The main difference may be related to a slight relaxation in the *Rc* position and a further small decrease in the free volume amount and size.

Starting from 460°C, the residual stresses start to relax, although the potassium surface concentration appears to steadily increase (Fig. 1). The relaxation at 460°C is still modest, becoming substantial at 490°C. There are several signatures of such stress relaxation on the medium-range structure.

(i) The free volume size and the average positron lifetime increase (Fig. 2). This points out that the structure starts to become more open and the amount of free space increases. The phenomenon is coupled with higher surface potassium concentration, which is expected to further increase the volume of the system. The residual stresses decrease implies that said volume expansion must be accommodated in the direction orthogonal to the surface, implying the existence of some viscous flow phenomena (time and temperature dependent).

(ii) The low-frequency portion of the *R* band increases its intensity (Fig. 3), suggesting the an increasing contribution associated with larger-ring environments (high Si-O-Si bond angle) able to accommodate the potassium ions. This evolution in the *R* band is a specific signature of the evolution of the silicate network, as it remained unchanged up to 430°C. We note that the said phenomenon is strictly related to the potassium incorporation and not to the thermal history the glass undergoes during IE, since the prevalence of the said big rings in the Raman spectra can be detected only on the surface of the IE glass (Fig. 5).

(iii) The *Rc* increases its intensity as a result of a re-ordering of the alkali-silicate-like regions, which is thermally-activated.

(iv) The *Rc* band first slightly relaxes, decreasing by a few cm^{-1} at 460°C; when the stress starts to drop at 490°C, the *Rc* return to its original position. The stress relaxation can appear, therefore, strongly connected to a change in the local configuration of the bonding angles. We note that the driving force for the relaxation of the residual stresses via viscous flow is not just the stored elastic energy ($u = \sigma^2/2E$, σ being the stress), but a chemical contribution must also be present. This chemical driving force includes the free energy difference between the relaxed and unrelaxed network, these being characterized by the said differences in the bond angles and free volume size. This excess energy, stored in the strained silicate network, may provide an additional driver for the relaxation phenomena.

We can finally highlight that similar patterns in the vibrational features and PALS spectra are observed on both air and tin sides of the float glass, thus indicating comparable structural changes. Nevertheless, it is important to note that the tin side is consistently denser (with lower free volume size and amount) due to the presence of tin atoms. In addition, relaxation phenomena appear slightly faster on the air side in terms of residual stresses (Fig. 1(e)), which can be attributed to a slightly quicker increase in the average positron lifetime above 430°C.

5. Conclusions

The medium range of the glass network evolves substantially during IE. Increasing the process temperature, the following phenomena are observed:

i. At 380°C, potassium ions can sit in thermodynamically favorable sites that can fit without inducing a deformation of the silicate network. When this occurs, the free volume size and amount decrease, and part of the theoretical residual stresses can be relaxed by a time/temperature-independent mechanism associated with an increase in the packing factor of the solid.
ii. When the temperature exceeds 400°C, further potassium incorporation may cause a network deformation, squeezing the Si-O-Si bonding angles in the alkali-silicate-like regions (*Rc* Raman band). A progressive reduction in free volume is observed.
iii. At 430°C, the maximum residual stress can be achieved, corresponding to a minimum in the size and amount of the free volume.
iv. Starting from 460°C, the network relaxes, increasing the amount and size of the free volume, ordering and re-organizing the bond angles in the alkali-silicate-like regions (*Rc* Raman band), forming larger silicate rings (*R* Raman band). This medium-range evolution must be coupled with viscous flow and is associated with a decrease in the residual stresses. Specifically, two well-defined configurations in the bonding angles (*Rc* Raman band) are shown, whose relaxation to the equilibrium couples with an abrupt drop in the residual stresses.

The discussed dynamics were observed both on the air and the tin side of the float glass with minor differences.

Finally, it is inferred that the free energy excess in the strained silicate network (lower Si-O-Si bond angles and free volume) can provide an additional chemical contribution to the relaxation phenomena beyond the mere elastic energy.

CRediT authorship contribution statement

Mattia Biesuz: Writing – original draft, Visualization, Supervision, Methodology, Investigation, Funding acquisition, Conceptualization. **Michele Cassetta:** Validation, Investigation. **Levent Karacasulu:** Software, Investigation, Data curation. **Adane M. Abebe:** Investigation. **Maciej Oskar Liedke:** Writing – review & editing, Validation. **Ahmed G. Attallah:** Writing – review & editing, Validation. **Eric Hirschmann:** Writing – review & editing, Validation. **Andreas Wagner:** Writing – review & editing, Supervision. **Sebastiano Mariazzi:** Investigation. **Roberto S. Brusa:** Writing – review & editing, Validation, Supervision. **Vincenzo M. Sglavo:** Writing – review & editing, Validation, Supervision, Resources.

Declaration of competing interest

The authors declare that they have no known competing financial interests or personal relationships that could have appeared to influence the work reported in this paper.

Acknowledgements

Parts of this research were carried out at ELBE at the Helmholtz-Zentrum Dresden – Rossendorf e. V., a member of the Helmholtz Association. We would like to thank the facility staff for assistance. The authors would like to thank the Centre for Technological Platforms (CPT) of the University of Verona (Italy) for providing access to scientific instrumentation and technical support.

Mr. Alessandro Tomasini and Enrico Kambo are warmly acknowledged for the technical support.

Appendix A. Supplementary data

Supplementary Materials including additional EDX and SIMS characterization data. Supplementary data to this article can be found online at https://doi.org/10.1016/j.apsusc.2026.167948.

Data availability

Data will be made available on request.

References

[1] J.E. Shelby, Introduction to Glass Science and Technology, second ed., The Royal Society of Chemistry, Cambridge, 2005.
[2] A.K. Varshneya, Fundamentals of inorganic glasses, Academic Press, Inc., 1994. https://doi.org/10.1016/0022-3093(94)90112-0.
[3] G.D. Sorarù, S. Mariazzi, M. Barozzi, R. Canteri, M. Cassetta, D. Pellegrini, N. Daldosso, R.S. Brusa, M. Biesuz, On the structure and properties of hydrothermally toughened soda–lime silicate float glass, J. Am. Ceram. Soc. 107 (2024) 5383–5399, https://doi.org/10.1111/jace.19832.
[4] M. Krohn, J.R. Hellmann, C.G. Pantano, N. Lower, R.K. Brow, Effects of tin on the physical properties and crack growth in soda-lime-silica float glass, Key Eng. Mater. 264–268 (2004) 1859–1862, https://doi.org/10.4028/www.scientific.net/KEM.264-268.1859.
[5] L. Jiang, X. Guo, X. Li, L. Li, G. Zhang, Y. Yan, Different K^+–Na^+ inter-diffusion kinetics between the air side and tin side of an ion-exchanged float aluminosilicate glass, Appl. Surf. Sci. 265 (2013) 889–894, https://doi.org/10.1016/j.apsusc.2012.11.143.
[6] X. Li, L. Jiang, Y. Wang, I. Mohagheghian, J.P. Dear, L. Li, Y. Yan, Correlation between K^+-Na^+ diffusion coefficient and flexural strength of chemically tempered aluminosilicate glass, J. Non Cryst. Solids 471 (2017) 72–81, https://doi.org/10.1016/j.jnoncrysol.2017.05.011.
[7] R.A. Synowicki, B.D. Johs, A.C. Martin, Optical properties of soda-lime float glass from spectroscopic ellipsometry, Thin Solid Films 519 (2011) 2907–2913, https://doi.org/10.1016/j.tsf.2010.12.110.
[8] M. Biesuz, G. Mariotto, M. Cassetta, O. Ersen, D. Ihiawakrim, P. Haušild, P. Giopato, A. Martucci, M. Bortolotti, V.M. Sglavo, G.D. Sorarù, Solid-state field-assisted ion exchange (Ag → Na) in soda–lime float glass: tin versus air side, Adv. Eng. Mater. 25 (2023) 2201572, https://doi.org/10.1002/adem.202201572.
[9] A. Mareska, Formation of silver colloids on the tin side of the float glass, Ceram. Silik. (2023) 348–359. https://doi.org/10.13168/cs.2023.0035.
[10] J.A. Howell, J.R. Hellmann, C.L. Muhlstein, Nanomechanical properties of commercial float glass, J. Non Cryst. Solids 354 (2008) 1891–1899, https://doi.org/10.1016/j.jnoncrysol.2007.10.021.
[11] O. Goodman, B. Derby, The mechanical properties of float glass surfaces measured by nanoindentation and acoustic microscopy, Acta Mater. 59 (2011) 1790–1799, https://doi.org/10.1016/j.actamat.2010.11.045.
[12] M.H. Krohn, J.R. Hellmann, B. Mahieu, C.G. Pantano, Effect of tin-oxide on the physical properties of soda-lime–silica glass, J. Non Cryst. Solids 351 (2005) 455–465, https://doi.org/10.1016/j.jnoncrysol.2005.01.050.
[13] S. Bornemann, S. Henning, K. Naumenko, M. Pander, N. Thavayogarajah, M. Würkner, Strength analysis of laminated glass/EVA interfaces: microstructure, peel force and energy of adhesion, Compos. Struct. 297 (2022) 115940, https://doi.org/10.1016/j.compstruct.2022.115940.
[14] H. He, H. Liu, Y. Lin, C. Qu, J. Yu, S.H. Kim, Differences in indentation and wear behaviors between the two sides of thermally tempered soda lime silica glass, J. Am. Ceram. Soc. 104 (2021) 4718–4727, https://doi.org/10.1111/jace.17872.
[15] S.S. Kistler, Stresses in glass produced by nonuniform exchange of monovalent ions, J. Am. Ceram. Soc. 45 (1962) 59–68, https://doi.org/10.1111/j.1151-2916.1962.tb11081.x.
[16] P. Acloque, J. Tochon, Measurement of Mechanical Resistance of Glass after Reinforcement, in: Colloquium on Mechanical Strength of Glass and Ways of Improving It, September 25–29, 1961, Florence Italy. Union Scientifique Continentale Du Verre, Charlroi, Belgium, 1962: pp. 687–704.
[17] A.K. Varshneya, Chemical strengthening of glass: lessons learned and yet to be learned, Int. J. Appl. Glass Sci. 1 (2010) 131–142, https://doi.org/10.1111/j.2041-1294.2010.00010.x.
[18] D.A. Krohn, A.R. Cooper, Strengthening of Glass Fibers: I, Cladding, J. Am. Ceram. Soc. 52 (1969) 661–664, https://doi.org/10.1111/j.1151-2916.1969.tb16072.x.
[19] A.K. Varshneya, Fundamentals of inorganic glasses, Academic Press, Inc., 1994. https://doi.org/10.1016/0022-3093(94)90112-0.
[20] O. Banapour Ghaffari, B. Eftekhari Yekta, M. Zakeri-Nasrabadi, Estimating "depth of layer" (DOL) in ion-exchanged glasses using explainable machine learning, Materialia (Oxf) 33 (2024) 102027. https://doi.org/10.1016/j.mtla.2024.102027.
[21] O. Banapour Ghaffari, B. Eftekhari Yekta, M. Zakeri-Nasrabadi, Designing high-performance ion-exchangeable glasses with multi-objective optimization and machine learning, Ceram. Int. 50 (2024) 42949–42962. https://doi.org/10.1016/j.ceramint.2024.08.141.
[22] S. Barbi, C. Mugoni, M. Montorsi, C. Siligardi, Chemical hardening of glazed porcelain tiles, J. Ame. Ceram. Soc. 102 (2018) jace.16134, https://doi.org/10.1111/jace.16134.
[23] M. Dal Bó, A. Zimmer, S.R. Grando, P. Kaspari, D. Hotza, Increase mechanical strength in porcelain stoneware tile by ion exchange, Boletín De La Sociedad Española De Cerámica y Vidrio 55 (2016) 197–201, https://doi.org/10.1016/j.bsecv.2016.06.001.
[24] C. Dauber, M. Dal Bó, D. Hotza, A.K. Alves, Use of chemically tempered porcelain tiles in ballistic protection, Ceram. Int. 49 (2023) 5550–5556, https://doi.org/10.1016/j.ceramint.2022.11.287.
[25] B. Nascimento de Souza, M. Dal Bó, D. Hotza, M.C. Fredel, Chemical modification of porcelain tile surface to optimize flexural strength and Weibull modulus through the ion exchange process, J. Build. Eng. 56 (2022) 104735, https://doi.org/10.1016/j.jobe.2022.104735.
[26] X.C. Li, M. Meng, D. Li, R. Wei, L. He, S.F. Zhang, Strengthening and toughening of a multi-component lithium disilicate glass-ceramic by ion-exchange, J. Eur. Ceram. Soc. 40 (2020) 4635–4646, https://doi.org/10.1016/j.jeurceramsoc.2020.05.075.
[27] K. Łączka, K. Cholewa-Kowalska, M. Środa, J. Rysz, M.M. Marzec, M. Łączka, Glass–ceramics of LAS (Li_2O-Al_2O_3-SiO_2) system enhanced by ion-exchange in KNO_3 salt bath, J. Non Cryst. Solids 428 (2015) 90–97, https://doi.org/10.1016/j.jnoncrysol.2015.08.003.
[28] K.D. Vargheese, A. Tandia, J.C. Mauro, Molecular dynamics simulations of ion-exchanged glass, J. Non Cryst. Solids 403 (2014) 107–112. https://doi.org/10.1016/j.jnoncrysol.2014.07.025.
[29] M. Wang, B. Wang, N.M.A. Krishnan, Y. Yu, M.M. Smedskjaer, J.C. Mauro, G. Sant, M. Bauchy, Ion exchange strengthening and thermal expansion of glasses: common origin and critical role of network connectivity, J. Non Cryst. Solids 455 (2017) 70–74. https://doi.org/10.1016/j.jnoncrysol.2016.10.027.
[30] C. Ragoen, M.A.T. Marple, S. Sen, T. Lambricht, S. Godet, Structural modifications induced by Na^+/K^+ ion exchange in silicate glasses: a multinuclear NMR spectroscopic study, J. Non Cryst. Solids 474 (2017) 9–15. https://doi.org/10.1016/j.jnoncrysol.2017.08.006.
[31] N. Terakado, R. Sasaki, Y. Takahashi, T. Fujiwara, S. Orihara, Y. Orihara, A novel method for stress evaluation in chemically strengthened glass based on micro-Raman spectroscopy, Commun. Phys. 3 (2020) 37, https://doi.org/10.1038/s42005-020-0305-7.
[32] N. Terakado, S. Uchida, Y. Takahashi, T. Fujiwara, M. Arakawa, Depth analysis of a compression layer in chemically strengthened glass using depth-resolved micro-Raman spectroscopy, J. Ceram. Soc. Jpn. 124 (2016) 1164–1166, https://doi.org/10.2109/jcersj2.16138.
[33] C. Calahoo, J.W. Zwanziger, I.S. Butler, Mechanical–structural investigation of ion-exchanged lithium silicate glass using Micro-Raman spectroscopy, J. Phys. Chem. C 120 (2016) 7213–7232, https://doi.org/10.1021/acs.jpcc.6b01720.
[34] A.K. Varshneya, The physics of chemical strengthening of glass: Room for a new view, J. Non Cryst. Solids 356 (2010) 2289–2294, https://doi.org/10.1016/j.jnoncrysol.2010.05.010.
[35] A.K. Varshneya, G.A. Olson, P.K. Kreski, P.K. Gupta, Buildup and relaxation of stress in chemically strengthened glass, J. Non Cryst. Solids 427 (2015) 91–97, https://doi.org/10.1016/j.jnoncrysol.2015.07.037.

[36] G. Macrelli, A.K. Varshneya, J.C. Mauro, Simulation of glass network evolution during chemical strengthening: resolution of the subsurface compression maximum anomaly, J. Non Cryst. Solids 522 (2019) 119457, https://doi.org/10.1016/j.jnoncrysol.2019.05.033.
[37] M. Biesuz, M. Cipriani, V.M. Sglavo, G.D. Sorarù, Electrode-dependent Joule heating in soda lime silicate glass during flash processes, Scr. Mater. 182 (2020) 94–98, https://doi.org/10.1016/j.scriptamat.2020.03.005.
[38] A. Wagner, M. Butterling, M.O. Liedke, K. Potzger, R. Krause-Rehberg, Positron annihilation lifetime and Doppler broadening spectroscopy at the ELBE facility, AIP Conf. Proc. (2018) 040003, https://doi.org/10.1063/1.5040215.
[39] E. Hirschmann, M. Butterling, U. Hernandez Acosta, M.O. Liedke, A.G. Attallah, P. Petring, M. Görler, R. Krause-Rehberg, A. Wagner, A new system for real-time data acquisition and pulse parameterization for digital positron annihilation lifetime spectrometers with high repetition rates, J. Instrum. 16 (2021) P08001, https://doi.org/10.1088/1748-0221/16/08/P08001.
[40] J.V. Olsen, P. Kirkegaard, N.J. Pedersen, M. Eldrup, PALSfit: a new program for the evaluation of positron lifetime spectra, Phys. Status Solidi C 4 (2007) 4004–4006, https://doi.org/10.1002/pssc.200675868.
[41] M. Zanatta, G. Baldi, R.S. Brusa, W. Egger, A. Fontana, E. Gilioli, S. Mariazzi, G. Monaco, L. Ravelli, F. Sacchetti, Structural evolution and medium range order in permanently densified vitreous SiO_2, Phys. Rev. Lett. 112 (2014) 45501, https://doi.org/10.1103/PhysRevLett.112.045501.
[42] T.L. Dull, W.E. Frieze, D.W. Gidley, J.N. Sun, A.F. Yee, Determination of pore size in mesoporous thin films from the annihilation lifetime of positronium, J. Phys. Chem. B 105 (2001) 4657–4662, https://doi.org/10.1021/jp004182v.
[43] M. Cassetta, M. Zanatta, M. Biesuz, M. Giarola, G. Mariotto, New insights about the role of Na–K ratio on the vibrational dynamics of synthetic-basalt glasses, J. Raman Spectrosc. (2022), https://doi.org/10.1002/jrs.6298.
[44] M. Biesuz, L. Karacasulu, M. Cassetta, M. Barozzi, R. Canteri, M.O. Liedke, E. Hirschmann, A. Wagner, S. Mariazzi, G.D. Sorarù, V.M. Sglavo, R.S. Brusa, On the asymmetry of soda lime silicate float glass structure and chemistry, J. Am. Ceram. Soc. 109 (2026), https://doi.org/10.1111/jace.70488.
[45] A. Rahman, G. Mariotto, E. Cattaruzza, E. Trave, F. Gonella, A. Quaranta, Thermal annealing and laser induced structural rearrangement and silver state modification in Ag^+-Na^+ ion-exchanged silicate glasses studied by Raman spectroscopy, J. Non Cryst. Solids 552 (2021) 120455, https://doi.org/10.1016/j.jnoncrysol.2020.120455.
[46] T. Furukawa, K.E. Fox, W.B. White, Raman spectroscopic investigation of the structure of silicate glasses. III. Raman intensities and structural units in sodium silicate glasses, J. Chem. Phys. 75 (1981) 3226–3237, https://doi.org/10.1063/1.442472.
[47] R.B. Laughlin, J.D. Joannopoulos, Phonons in amorphous silica, Phys. Rev. B 16 (1977) 2942–2952, https://doi.org/10.1103/PhysRevB.16.2942.
[48] S. Ben Khemis, E. Burov, H. Montigaud, D. Skrelic, E. Gouillart, L. Cormier, Structural analysis of sputtered amorphous silica thin films: a Raman spectroscopy investigation, Thin Solid Films 733 (2021) 138811, https://doi.org/10.1016/j.tsf.2021.138811.
[49] B. Hehlen, D.R. Neuville, D. Kilymis, S. Ispas, Bimodal distribution of Si–O–Si angles in sodo-silicate glasses, J. Non Cryst. Solids 469 (2017) 39–44, https://doi.org/10.1016/j.jnoncrysol.2017.04.009.
[50] R.K. Biswas, P. Khan, S. Mukherjee, A.K. Mukhopadhyay, J. Ghosh, K. Muraleedharan, Study of short range structure of amorphous Silica from PDF using Ag radiation in laboratory XRD system, RAMAN and NEXAFS, J. Non Cryst. Solids 488 (2018) 1–9, https://doi.org/10.1016/j.jnoncrysol.2018.02.037.
[51] M. Cassetta, G.D. Sorarù, E. Callone, S. Dirè, A.M. Abebe, S. Mariazzi, R.S. Brusa, M. Giarola, N. Daldosso, M. Biesuz, From $SiO_{1.5}CH_3$ to vitreous SiO_2: a structural evolution study, J. Non. Cryst. Solids 648 (2025) 123327, https://doi.org/10.1016/j.jnoncrysol.2024.123327.
[52] İ. Erdem, D. Guldiren, S. Aydin, Chemical tempering of soda lime silicate glasses by ion exchange process for the improvement of surface and bulk mechanical strength, J. Non Cryst. Solids 473 (2017) 170–178, https://doi.org/10.1016/j.jnoncrysol.2017.08.010.
[53] V.M. Sglavo, P. Bettotti, E. Callone, S. Dirè, Chemical strengthening of float glasses: effect of composition and structure, J. Am. Ceram. Soc. 109 (2026), https://doi.org/10.1111/jace.70317.
[54] G. Pintori, V.M. Sglavo, Electric-field assisted ion-exchange of innovative float glass, J. Non. Cryst. Solids (2022) in press.
[55] G. Macrelli, J.C. Mauro, A.K. Varshneya, Coupling of diffusion and chemical stress: the case of ion exchange in glass, J. Am. Ceram. Soc. 104 (2021) 5599–5613, https://doi.org/10.1111/jace.17926.
[56] C. Ragoen, L. Cormier, A.-I. Bidegaray, S. Vives, F. Henneman, N. Trcera, S. Godet, A XANES investigation of the network-modifier cations environment before and after the Na^+/K^+ ion-exchange in silicate glasses, J. Non Cryst. Solids 479 (2018) 97–104, https://doi.org/10.1016/j.jnoncrysol.2017.10.021.
[57] O. Majérus, L. Cormier, G. Calas, B. Beuneu, A neutron diffraction study of temperature-induced structural changes in potassium disilicate glass and melt, Chem. Geol. 213 (2004) 89–102, https://doi.org/10.1016/j.chemgeo.2004.08.035.
[58] W.E. Jackson, G.E. Brown, C.W. Ponader, X-ray absorption study of the potassium coordination environment in glasses from the $NaAlSi_3O_8$-$KAlSi_3O_8$ binary, J. Non Cryst. Solids 93 (1987) 311–322, https://doi.org/10.1016/S0022-3093(87)80177-1.